Scanning Microscopy

Volume 2 | Number 4 Article 14

8-12-1988

# Scanning Electron Microscopy Studies of Extended Defects in Semiconductors

C. A. Dimitriadis
*University of Thessaloniki*

Scanning Microscopy, Vol. 2, No. 4, 1988 (Pages 1979-1993)
Scanning Microscopy International, Chicago (AMF O'Hare), IL 60666 USA

0891-7035/88$3.00+.00

# SCANNING ELECTRON MICROSCOPY STUDIES OF EXTENDED DEFECTS IN SEMICONDUCTORS

C.A. Dimitriadis

Department of Physics. Solid State Section 313-1,
University of Thessaloniki, Thessaloniki 54006, Greece

(Received for publication January 29, 1988, and in revised form August 12, 1988)

## Abstract

Extended defects, such as dislocations and grain boundaries, play an important role in determining the performance of various semiconductor devices. This paper reviews applications of electron-beam-induced-current and cathodoluminescence scanning electron microscopy for the investigation of dislocations and grain boundaries in semiconductors. We developed a simple analytical method for the determination of the grain boundary recombination velocity and the minority carrier diffusion length, in contrast to a previous method which requires the use of a computer for the numerical calculation of an integral expression. We, also, studied theoretically the influence of an individual dislocation on the minority carrier lifetime. Investigation of dislocations in GaP indicated that the carrier recombination takes place at a Cottrell atmosphere of the S-donor/Cu complexes surrounding the dislocations.

KEY WORDS: SEM, dislocations, grain-boundaries, semiconductor.

## Introduction

Minority carrier diffusion length(L) and lifetime($\tau$) are important parameters which determine the performance of various semiconductor devices. Extended defects, such as dislocations and grain boundaries(GBs) in polycrystalline semiconductors, affect the parameters L and $\tau$ (Dimitriadis,1985a, 1985b, 1986) and, therefore, characterization of these defects is of great importance for device applications. Scanning electron microscopy (SEM) in the electron-beam-induced-current(EBIC) and cathodoluminescence(CL) modes of operation is well suited for characterization of defects in semiconductors and semiconductor devices. A number of text books give the basic principles of an SEM (Thornton, 1968; Oatley, 1972; Holt et al., 1974).

The finely focused electron-beam of the SEM acts as a localized source of excess carriers in the semiconductor. If the semiconductor contains an internal field (p-n junction or Schottky diode) part of the injected electrons and holes are collected by the junction field and produce a current in the external circuit. By scanning the electron beam across the semiconductor surface and forming an image using the EBIC signal, the presence of electrically active defects can be resolved (Leedy, 1977). Also, SEM-EBIC techniques were modelled for diffusion length and lifetime measurements(Berz and Kuiken,1976; Kuiken,1976;Leedy, 1977; Ioannou and Dimitriadis,1982) and characterization of grain boundaries(Zook,1980; Donolato and Klann,1980; Seager,1982; Burk et al., 1983; Donolato,1983; Dimitriadis,1985c).

In cases where the radiative recombination efficiency of the semiconductor is reasonably high, defects could also be detected by the CL mode. Many papers in the CL area appeared in the last few years. Most of them dealt with CL measurements performed under steady-state conditions and only recently were time-dependent measurements reported for lifetime measurements in a dislocation-free area of the sample (Davidson and Dimitriadis,1980; Steckenborn,1980;Steckenborn et al., 1981; Hastenrath and Kubalek,1982; Myhajlenko and Ke,1984) and in the vicinity of an individual dislocation (Rasul and Davidson,1977; Dimitriadis et al,,1978; Dimitriadis,1983). A theoretical treatment of time-dependent CL in a

dislocation-free area of the sample was repoted recently (Jakubowicz,1987). To the author's knowledge time-dependent CL in the vicinity of an individual dislocation has not been treated so far.

An advantage of the CL method is that the only sample preparation needed for CL work is polishing of the surface to be studied, while in the EBIC method heat treatment for device fabrication may change the characteristics of the starting material. Therefore, for assessment of the starting material, the CL method is more suitable for materials of high luminescence efficiency and the EBIC method for materials of low luminescence efficiency.

Here we are mainly concerned with recent developments and advances in EBIC and CL techniques for the investigation of extended defects in semiconductors. Several authors have measured the GB recombination velocity in Si bicrystals by applying quantitative EBIC methods (Burk et al.,1983; Donolato,1983; Seager,1982). Their quantitative analysis of the induced current profile at a GB requires the use of a computer for numerical calculation of an integral expression. In contrast to previous authors, we derived a simple analytical expression for the EBIC profile at a GB for point source excitation (Dimitriadis,1985c). Based on this expression, the GB recombination velocity and the diffusion length in the grain can be, easily, obtained by fitting the experimental and theoretical induced-current profiles.

Also, this work presents a theoretical analysis of the CL signal after switching off the electron beam in the vicinity of an individual dislocation. From the analysis of the CL decay when the electron beam is located at various distances from the dislocation, the influence of the dislocation on the minority carrier lifetime can be determined. By studying the influence of a single dislocation on the bulk lifetime, the dislocation recombination process can be resolved. Practical application of this technique indicated that carrier recombination at dislocations in GaP is due to a Cottrell atmosphere of the S-donor/Cu complexes segregated around the dislocations (Dimitriadis,1983, 1985a, 1985b).

## Carrier Generation and Recombination

### Generation

The EBIC and CL modes of SEM operation rely on the generation of excess minority carriers by the electron beam:The electron beam impinging on the semiconductor undergoes a successive series of elastic and inelastic scattering mechanisms. As a result of these scattering events in the semiconductor, the electron beam transfers its energy to the lattice electrons over a distance given by the Gruen expression

$$R_e=(k/\rho)E_b^n \qquad (1)$$

where $E_b$ is the electron beam energy, $\rho$ is the density of the material, k and n are constants which depend on the atomic number of the material (Z) and the electron beam energy ($E_b$). According to Everhart and Hoff (1971), for electron energy range $5<E_b<25$keV and atomic numbers $10<Z<15$, the range of electron penetration ($R_e$) is given by

$$R_e=(0.0398/\rho)E_b^{1.75} \ (\mu m) \qquad (2)$$

where $\rho$ is in $g/cm^3$ and $E_b$ is in keV. Kanaya and Okayama (1972) derived a more general expression for $R_e$ for a wider range of atomic numbers.According to Kanaya and Okayama (1972) the range $R_e$ is given by

$$R_e=(0.027A/\rho Z^{0.889})E_b^{1.65} \ (\mu m) \qquad (3)$$

where A is the atomic weight in g/mol, $\rho$ is in $g/cm^3$ and $E_b$ is in keV. The shape of the generation volume depends on the atomic number. For material of low atomic number the generation volume is pear-shaped, for $15<Z<40$ the generation volume is spherical and for larger atomic numbers the generation volume is hemispherical.

The electron-hole pair generation rate (G) is given by

$$G=\frac{V_b I_b}{qE_i}(1-\varepsilon)=\frac{V_b I_b Q}{qE_g}(1-\varepsilon) \qquad (4)$$

where $V_b$ and $I_b$ are the electron beam voltage and energy, respectively, q is the electronic charge, $E_i$ is the ionization energy (i.e. the energy required for the formation of an electron-hole pair), $E_g$ is the energy band gap, Q is the quantum-efficiency for electron-hole pair generation and $\varepsilon$ is the fraction of the electron beam energy lost due to backscattered electrons. Q is typically 30% for many semiconductors, showing that this fraction of the electron beam energy generated carriers, while the remainder energy is dissipated as heat. The ionization energy $E_i$ depends on the band gap of the semiconductor according to the relationship $E_0=2.8E_g+M$ where $0<M<1$eV.

### Recombination

The charge carriers generated as described above will be subjected to diffusion before recombination takes place. The three factors of generation, diffusion and recombination determine the three-dimensional distribution of the excess minority carriers. Under steady-state conditions, the differential equation giving the spatial distribution for a n-type semiconductor is:

$$D\nabla^2\Delta p - \frac{\Delta p}{\tau} + G = 0 \qquad (5)$$

where $\Delta p$ is the concentration of excess holes, D is the hole diffusion coefficient,$\tau$ is the hole lifetime and G is the generation function mentioned above. When the diffusion length L is significantly larger than the generation volume radius, then the assumption of a point source excitation can be made. This assumption simplifies the problem of finding a solution of the diffusion equation.

Various boundary conditions should be taken into account when solving Eq. (5). Surface recombination becomes an important factor limiting the excess carrier density, because the carriers will mostly be generated within a diffusion length of the surface and most of the carriers reaching the surface will recombine there. If s is the surface recombination velocity, the solution of Eq. (5) must satisfy the boundary condition

$$D \left.\frac{\partial \Delta p}{\partial z}\right|_{z=0} = s\Delta p|_{z=0} \qquad (6)$$

Also, if other recombination processes take place, additional boundary conditions should be considered. Here, we are mainly concerned with recombination at dislocations and grain boundaries. In case where the semiconductor surface contains a rectifying contact, the surface recombination velocity can be considered as infinite and the boundary condition (6) becomes

$$\Delta p|_{z=0} = 0 \qquad (7)$$

In the following sections, for investigation of dislocations and grain boundaries, we describe SEM-EBIC and CL methods based on the solution of Eq. (5) with the appropriate boundary conditions.

## SEM Investigation of Dislocations in Semiconductors

### Dislocation density

For semiconductors of high luminescence efficiency, the CL mode of the SEM has been used for measurement of the dislocation density. The EBIC mode of the SEM can also be used and is indeed necessary for non-luminescence semiconductors such as silicon. The CL technique has the advantage that it allows measurements to be performed without sample preparation to form rectifying and ohmic contacts. Under most circumstances both methods rely on the local reduction of the minority carrier lifetime corresponding to a decrease in the CL or EBIC signal (Davidson and Dimitriadis, 1980).

In the EBIC methods, the p-n junction could be a more reliable rectifying contact than the Schottky barrier, because the junction is well below the surface and defects lying deep in the semiconductor could be detected. However, the fabrication of the p-n junction involves high temperature process, diffusion or epitaxy, which may modify the dislocation concentration and distribution in the material, and therefore defects observed in the EBIC image might not be representative of the original material. The Schottky barrier EBIC method does not suffer from this limitation since room temperature process is required for fabrication of the rectifying contact, but great care must be taken in the sample preparation for the formation of good Schottky barriers.

SEM-EBIC Schottky barrier and CL micrographs from the same area of the specimen show that there is 1:1 correspondence between dark dots in the two types of micrographs. Typical EBIC Schottky barrier and CL micrographs, obtained from the same area of a LPE GaP layer, are illustrated in Fig. 1. The CL micrographs also include some dark lines, not observed in the EBIC micrographs. These lines can be explained as due to a corrugated or lamellar surface structure which is obtained in epilayers grown in the LPE process. The dark lines in the CL micrograph could be a result of the smaller extraction of the internally generated light from these steps on the specimen surface.

The spatial resolution of the EBIC or CL mode is generally determined by three factors:the electron-probe size, the generation volume radius $r_g$ and the minority carrier diffusion length L.In

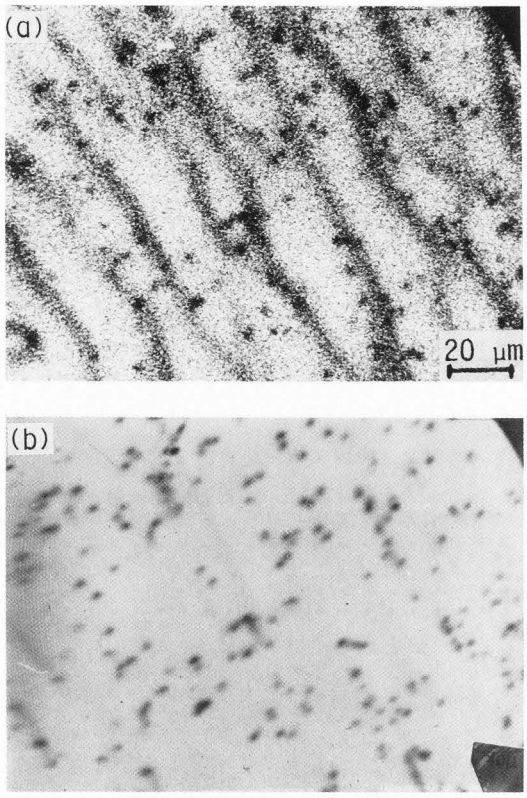


FIG. 1 One to one correspondence between black dots in (a) CL and (b) EBIC micrographs obtained from the same area of a GaP sample ($E_b$=25 keV).

practice the same beam spot size varies between 0.5 to 1 μm which is smaller than the generation volume at electron energies between 7.5 to 25 keV and, thereby, not limiting the resolution. When the diffusion is large, the carriers diffuse a significant distance before recombining, the resolution should decrease and the micrograph become more blurred. The resolution is expected to be determined by a parameter resulting from adding the generation volume radius and diffusion length in quadrature (Davidson,1977). In general, the experimental resolution appears to be rather better, particularly in the EBIC mode, than the expected resolution. One possible explanation for this is that, close to the surface, the value of L should be reduced due to high recombination at the top surface and the resolution should be determined only by the generation volume.

From Fig.1(b) it is seen that the diameter of the black dots is about 5 to 6 μm and their density $\sim 4\times10^5$ cm$^{-2}$. However, the EBIC image resolution varies with the electron beam voltage. Fig.2 shows EBIC micrographs of the same sample region in a LPE GaP layer obtained at beam energy 25 keV and 15 keV, beam current $\sim 5\times10^{-8}$ A and beam diameter $\sim$1 μm. The black dot diameter in the EBIC micrographs reduces from about 5 μm for $E_b$=25 keV, to about 2 μm for $E_b$=15 keV. It is observed that the diameter of the black dots is about equal to that of the corresponding generation volume.Since

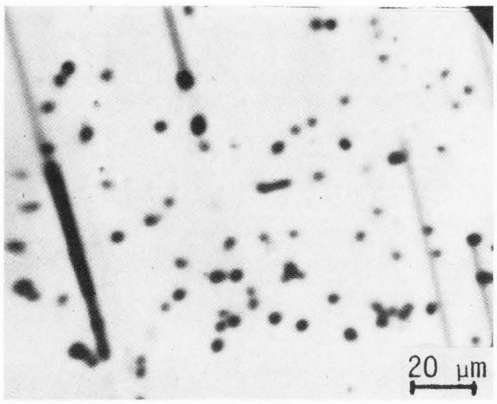


(a)
$E_b$=25keV

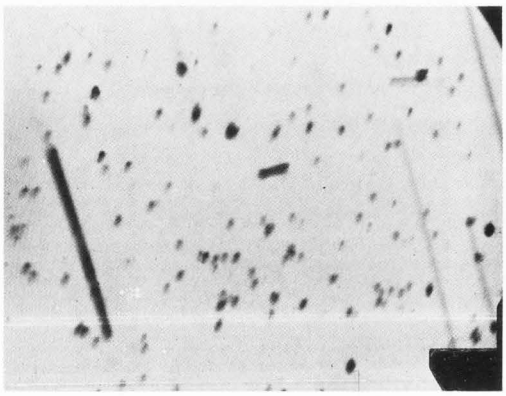

(b)
$E_b$=15keV

FIG.2 EBIC micrographs obtained from the same area of a GaP sample for different electron beam energies.

the diffusion length L>2µm, it is concluded that the EBIC image resolution of dislocations is not limited by the diffusion length but is solely determined by the generation volume. Therefore, when SEM is operated in the EBIC or CL mode, a compromise between signal/noise ratio and spatial resolution must be achieved for good quality EBIC or CL micrographs. The smallest electron energy must be compatible with the minimum detectable signal and the best resolution of the EBIC or CL mode.

Electrical Activity of Dislocations:The EBIC Method

A steady-state EBIC method has been used for investigation of dislocations in semiconductors. The geometrical configuration of the method is illustrated in Fig.3. A Schottky contact or a shallow p-n junction is applied for charge collection. The electron beam of the SEM penetrates the rectifying contact and generates electron-hole pairs in the semiconductor. The beam-generated carriers, which reach by diffusion the contact, are separated and collected by the built-in field producing an EBIC current in the external circuit. This current is used as video signal of the SEM.

When the probing beam approaches the dislocation, the collected current decreases as a result of the enhanced carrier recombination and contrast is produced at the screen of the SEM. A simple analytical description of the dislocation contrast

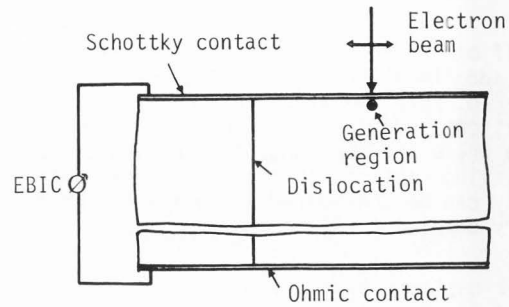


FIG.3 Schematic illustration of the experimental arrangement used for EBIC investigation of defects.

formation in the EBIC imaging has been published (Donolato,1979; Donolato and Klann,1980). The dislocation is represented as a continuous distribution of point defects on a semi-infinite line with the origin on the surface. First, Donolato (1978) obtained an analytical expression for the contrast profile (i.e., the ratio of the EBIC signal measured for the beam spot being located at the defect to the background current) of a point-like defect located at a depth z=H,

$$i^* = i^*(\xi, R_e, H, L, \gamma) \qquad (8)$$

$\xi$ being the beam position relative to the point defect, L the minority carrier diffusion length and $\gamma$ a constant giving the strength of the defect. The theoretical analysis was based on the assumptions: (a) the recombination rate at the defect is higher than in the bulk;(b) the influence of the defect on the minority carrier diffusion is treated as a perturbation; (c) the generation volume is a uniform sphere of radius equal to the half of the primary electron range ($R_e$) and tangent to the surface.

In the case of a straight dislocation perpendicular to the surface, the contrast profile of a dislocation $i_D$ was found by integrating Eq.(5)

$$i_D^*(\xi, R_e, H, L, \gamma) \propto \int_0^\infty i^*(\xi, R_e, H, L, \gamma)\, dH \qquad (9)$$

The dislocation contrast profile can be obtained by numerical calculation of the integral in the relationship (9). Then, by fitting the experimental data with the theoretical results, the minority-carrier diffusion length and the dislocation strength can be calculated. The above analysis was, also, extended for a straight semi-infinite dislocation with origin on the surface and inclined at a certain angle (Donolato and Klann,1980). Study of the contrast properties of a dislocation led to a simple practical criterion for deciding if the image feature corresponds to a dislocation or to a localized defect (Donolato,1979):if the black dot is evident at all beam energies, it corresponds to a line defect extending into the material; if it appears only for a definite beam energy $E_b$, it corresponds to a localized defect located at a depth about $R_e(E_b)/1.2$.

Recently, a time resolved EBIC method was modelled for investigation of dislocations in semiconductors (Jakubowicz,1985). The geometrical configuration of the method is illustrated in Fig.4.

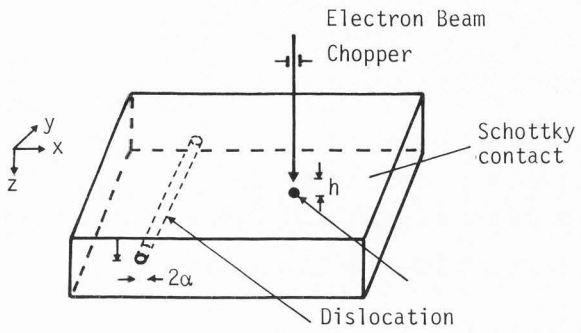


FIG.4 Schematic illustration of the time-resolved EBIC method used for investigation of a dislocation parallel to the sample surface.

The dislocation line is parallel to the charge collection plane at a depth H and is represented by a series of individual spheres of enhanced recombination. Each sphere corresponds to a pointlike defect which act as a sink for minority carriers and it has a strength characterized by an effective radius $\gamma\alpha$. The defect is characterized with "infinite strength" when $\gamma=1$ and with "finite strength" when $0\leq\gamma\leq1$.

Electron-hole pairs are generated by the electron beam which is switched off at t=0. Some of the carriers recombine at the dislocation and others are collected by the junction giving rise to an induced current in the external circuit. First, Jakubowicz (1985) obtained an analytical expression for the induced current decay with time in a semiconductor containing an individual pointlike defect. The source of electron-hole pairs was assumed to be pointlike located at a depth z=h and the injection level low. For a pointlike defect at a distance b from the source of excess carriers and for $\gamma\alpha<<b,H$, the current versus time relationship can be written as

$$I(t)=I_b(t)-I_d(t,h,H,b,L,\eta) \qquad (10)$$

where $\eta=\gamma\alpha/L$, $I_b(t)$ is the background current when the electron beam is positioned far from the defect and $I_d$ is the contribution of the defect to the collected current. This analysis, extended for a series of pointlike defects, can be used for characterization of individual dislocations in semiconductors. Thus, taking the sum over the whole length of the dislocation, the EBIC decay curves as a function of the parameter $\eta$ at a given distance $\chi$ of the point source from the dislocation can be written as

$$I(t)=I_o(t)-\sum_{\text{length}} I_d(t,h,\chi,L,\eta) \qquad (11)$$

where $I_o(t)$ is, as previously, the background current. When the electron beam is positioned far away from the dislocation ($\chi=\infty$), there is no influence of the dislocation on the EBIC decay curve (i.e, $\eta=0$). In this case, for long times t compared to lifetime $\tau$, the EBIC decays with time according to the relationship (Jakubowicz,1985)

$$I(t)\propto\exp(-t/\tau)/\ t^{3/2} \qquad (12)$$

Therefore, if $\ln(I\cdot t^{3/2})$ versus t is plotted, a straight line should result from the slope of which the lifetime can be obtained. When the electron beam is positioned close to the dislocation, the slope of the EBIC versus time plot is sensitive to the dislocation strength. By comparison of the experimental data with the theory, the strength of the dislocation as recombination centre can be determined. The above method can, also, be extended for a dislocation perpendicular to the surface or inclined at a certain angle.

Electrical Activity of Dislocations:The CL Method

CL studies in the SEM provide an excellent tool for characterizing the electrical activity of dislocations in semiconductors. Here, we present a theoretical analysis of the CL signal after switching off the electron beam in the vicinity of an individual dislocation. By comparison of the experimental data with the theoretical results, the bulk lifetime ($\tau_b$), the surface recombination velocity (s) and the effective dislocation core radius ($\alpha$) can be estimated.

CL Decay Near a Dislocation The geometrical arrangement of the experiment is shown in Fig.5.

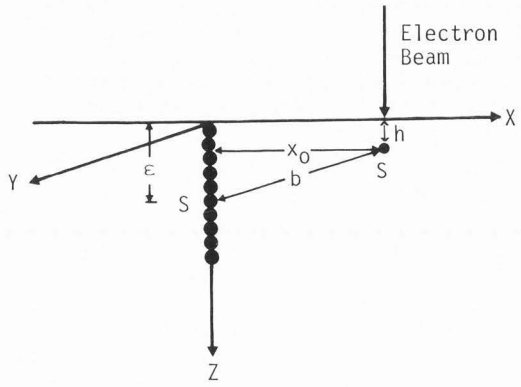


FIG.5 Schematic illustration of the model used for the study of the CL decay around a single dislocation.

Electron-hole pairs are generated by an electron beam which is switched off at time t=0. Some of the carriers diffusing away from the carrier source recombine at the surface and the dislocation, and others produce radiation in the whole volume of the material. In the analysis for the calculation of the total CL intensity, with the electron beam positioned near the dislocation, the following assumptions are made: (1) The sample surface is assumed to be semi-infinite i.e., bounded only by the top surface at z=0 which is characterized by a constant recombination velocity (s). (2) The diffusion length is much greater than the generation volume radius, i.e. we can consider excitation of a point source at a distance h below the surface. (3) The dislocation line is normal to the sample surface and it is represented by a series of pointlike defects. Each pointlike defect, acting as a sink for minority carriers, is considered to be a sphere with a characteristic effective

radius $\alpha$ (Jakubowicz,1985). If G is the strength of the point source, the pointlike defect at a depth $\xi$ acts as a sink with strength (Jakubowicz,1985)

$$G'=-(\alpha/b)\exp[(\alpha-b)/L]G \qquad (13)$$

where b is the distance between the defect and the source of excess carriers

$$b=\sqrt{X_o^2+(\xi-h)^2},\ \xi=n\alpha,\ n=1,3,5,... \qquad (14)$$

and $X_o$ is the distance between point source and dislocation. For derivation of Eq.(14) it was assumed that the pointlike defect is small enough, i.e. $b\gg\alpha$. (4) Self-absorption of the luminescence is negligible for semiconductor with an indirect gap like GaP. (5) The injected excess carrier density is small compared with the majority carrier density. Assuming that the local intensity of light produced by radiative recombination is proportional to the density of excess electron-hole pairs, the intensity I(t) of the total CL is given by

$$I(t)\sim\frac{1}{\tau_r}\int_{-\infty}^{\infty}\int_{-\infty}^{\infty}\int_{0}^{\infty}\Delta p(x,y,z)\,dx\,dy\,dz \qquad (15)$$

where $\tau_r$ is the radiative lifetime of the pairs and $\Delta p(x,y,z)$ is the local intensity of excess minority carriers (i.e., holes for n-type semiconductor).

In order to calculate the total population of excess minority carriers $(\Delta p)_{tot}$ at any time t, we will first calculate the total population of excess minority carriers $(\Delta p)_{tot,s}$ due to the point source S at a depth h and then we will consider the contribution of the point sink S' at a depth $\xi$. The contribution of the dislocation to the total population of excess minority carriers will be the sum of the point sinks over the whole length of the dislocation.

Von Roosbroeck (1955) has calculated the density of the excess minority carriers $\Delta p_s$ due to an instantaneous point source of unity strength, under the conditions stated at the beginning of this section. Using the results of Von Roosbroeck (1955) (Eq.22), we obtain the following expression for $\Delta p_s$:

$$\Delta p_s=G\tau(4\pi U)^{-3/2}\exp\left(-U-\frac{(X-X_o)^2+Y^2}{4U}\right)\exp(-U)\times$$
$$\times\left\{\exp\left[-\frac{(Z-H)^2}{4U}\right]+\exp\left[-\frac{(Z+H)^2}{4U}\right]-\right.$$
$$\left.2S\int_0^{\infty}\exp\left(-S\zeta-\frac{(Z+H+\zeta)}{4U}\right)d\zeta\right\} \qquad (16)$$

where U, $X_o$, X, Y, Z, H and S are dimensionless quantities defined by

$$U=t/\tau,\ X_o=x_o/L,\ X=x/L,\ Y=y/L$$
$$Z=z/L,\ H=h/L \text{ and } S=s/(L/\tau) \qquad (17)$$

$(\Delta p)_{tot,s}$ can now be obtained by integrating Eq. (16) over the entire sample volume. After some mathematical treatment, the final result is

$$(\Delta p)_{tot,s}=\frac{1}{2}(G/L^3)\exp(-U)\left[1+\mathrm{erf}\left(\frac{X_o}{2\sqrt{U}}\right)\right]\times$$
$$\times\left[1+\exp\{S(SU+H)\}\mathrm{erfc}\left(\frac{H}{2\sqrt{U}}+S\sqrt{U}\right)-\mathrm{erfc}\left(\frac{H}{2\sqrt{U}}\right)\right] \qquad (18)$$

where erf(x) and erfc(x) are the error and complementary error functions, respectively. Taking into account the contribution of the point sinks over the whole length of the dislocation, then by combining Eqs. (14) and (18) the total population of excess minority carriers is given by

$$(\Delta p)_{tot}=\frac{1}{2}(G/L^3)\times$$
$$\times\left[1-\exp(A)\sum_{n=1,3,5,..}\frac{\exp\left(-\sqrt{X_o^2+(nA-H)^2}\right)}{\sqrt{X_o^2+(nA-H)^2}}\right]\times$$
$$\times\left[1+\mathrm{erf}(X_o/2\sqrt{U}\right]\times\exp(-U)\times$$
$$\times\left[1+\exp\{S(SU+H)\}\mathrm{erfc}\left(\frac{H}{2\sqrt{U}}+S\sqrt{U}\right)-\right.$$
$$\left.-\mathrm{erfc}\left(\frac{H}{2\sqrt{U}}\right)\right] \qquad (19)$$

where A is the dimensionless quantity defined by $A=\alpha/L$. Therefore, the total CL intensity $I_N$ at any time t, normalized with respect to the CL intensity at t=0, is given by

$$I_N=\frac{I(t)}{I(0)}=$$
$$=\left\{1-A\exp(A)\sum_{n=1,3,5,..}\frac{\exp\left[-\sqrt{X_o^2+(nA-H)^2}\right]}{\sqrt{X_o^2+(nA-H)^2}}\right\}\times$$
$$\times\left\{1+\mathrm{erf}\left(\frac{X_o}{2\sqrt{U}}\right)\right\}\exp(-U)\times$$
$$\times\left\{1+\exp[S(SU+H)]\mathrm{erfc}\left(\frac{H}{2\sqrt{U}}+S\sqrt{U}\right)-\mathrm{erfc}\left(\frac{H}{2\sqrt{U}}\right)\right\} \qquad (20)$$

When the electron beam is positioned far from the dislocation there is no influence of the dislocation on the total population of excess minority carriers and using Eq. (18) the normalized CL intensity is

$$I_N=\exp(-U)\times$$
$$\times\left\{1+\exp[S(SU+H)]\mathrm{erfc}\left(\frac{H}{2\sqrt{U}}+S\sqrt{U}\right)-\mathrm{erfc}\left(\frac{H}{2\sqrt{U}}\right)\right\} \qquad (21)$$

First, we study the CL decay when the electron beam is positioned far from the dislocation. Equation (21) shows that the normalized CL decay, generally, has a non-exponential character. Using the asymptotic expansion of the complementary error function $\mathrm{erfc}(x)=\exp(-x^2)/\sqrt{\pi}\,x$ for $x\gg1$ (Abramowitz and Stegun,1965), then for large enough times the above expression of Eq. (21) can be simplified significantly to

$$I_N=\frac{\exp(-U)}{\sqrt{\pi US}} \qquad (22)$$

Therefore, for large t, plot of $\ln(I_N.\sqrt{t})$ versus t should give a straight line from the slope of which we can determine the minority carrier life-

time, i.e.

$$\tau = -1/\text{slope} \qquad (23)$$

The other parameter S can be determined by fitting the experimental $I_N(t)$ curves with their theoretical expression of Eq. (21).

When the electron beam is positioned near an infinitely long dislocation, then according to Eq. (20) the CL decay is influenced by the dislocation recombination (Fig. 6). For theoretical calculation of the curves $I_N(U)$ versus U, we consider that only part of the dislocation extending to a depth of about one diffusion length influence the CL decay. Since the parameter H is known and the parameters $\tau$ and S can be determined from the analysis of the CL decay when the electron beam is positioned far from the dislocation, by fitting the experimental curves $I_N(U)$ versus U with the Eq. (20), it should be able to determine the dislocation radius a. It is obvious that the sensitivity of the method will improve with decreasing the distance ($X_o$) of the beam from the dislocation. On the other hand, a limitation to the distance $x_o$ should be imposed since the method holds for $x_o >> a$. By studying the recombination efficiency of dislocations under various conditions, it will be possible to elucidate the recombination process at the dislocations.

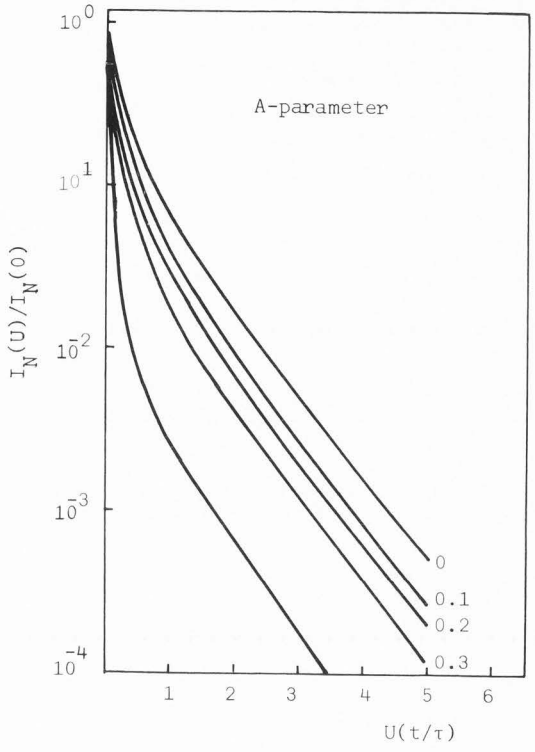


FIG. 6 Plot of the normalized CL against the normalized time U with the electron beam positioned at a distance $X_o$=1 from the dislocation; H=0.2, S=10 and S is a varying parameter.

Application: Recombination at Dislocation in GaP

The Recombination Process. In very pure semiconductors, like Si and Ge, spin-dependent effects indicated that the elementary centres of recombination at dislocations are most probably dangling bonds (Figielski,1978). Studies of the influence of dissociation of individual dislocations in Si into Schockleypartials on their carrier recombination efficiency, suggested that recombination at dislocations in Si is associated with their core-structure (Qurmazd and Booker,1978).However, the recombination process at dislocations in GaP was still unknown. Here, we summarize the attempt made to elucidate the dislocation recombination mechanism in GaP using the SEM-CL technique to measure the lifetime around single dislocations (Titchmarsh et al.1977;Dimitriadis et al.,1978; Dimitriadis,1983,1984b).

A SEM, substantially modified for efficient light collection (Davidson and Rasul,1977) was used for CL measurements. The luminescence was detected by a RCA C31024A photomultiplier, amplified and fed to a Brookdeal photon counting sampling unit. Electron beam blanking was achieved by modulating the Wehnelt cylinder. The response time of the system was about 3ns. The measurements were performed at 25 kV with beam current $5\times10^{-8}$A and electron probe diameter 1μm. The sample temperature could be varied between 77 and 500 K.

CL measurements were carried out on n-type liquid phase epitaxial (LPE) and vapour phase epitaxial (VPE) layers of GaP, doped with nitrogen at a concentration about $10^{18}$ $cm^{-3}$. Figure 7 shows typical CL decay curves with the beam located at a distance 6.7 μm from a dislocation and far from the dislocation in the sample LPE TH108.One clearly observes a reduction of the CL intensity as the electron beam approaches the dislocation and a rapid CL decay for small t followed by a

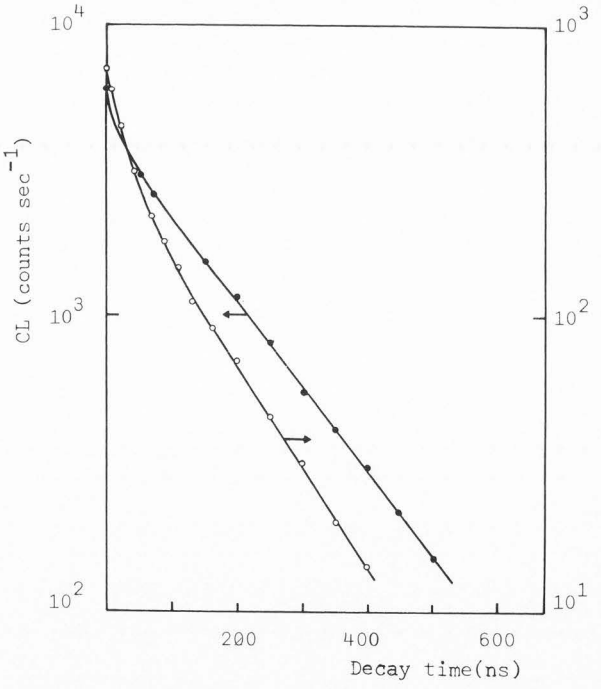


FIG. 7 Experimental CL decay curves with the electron beam positioned far from the dislocation (·) and at a distance 6.7 μm from the dislocation (○) and electron beam energy 25 keV.

near-exponential decay for large t, in agreement with our theoretical predictions. Also, the lifetime obtained from the time constant of the CL decay is reduced as the beam is positioned closer to the dislocation. Figure 8 shows the variation

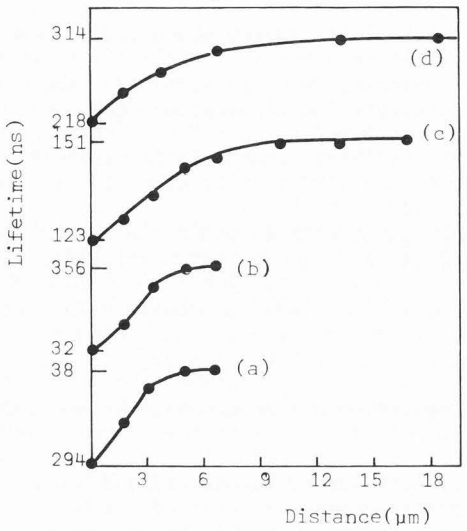


FIG. 8 Lifetime variation with distance from a dislocation in (a) green VPE, (b) VPE GPR217, (c) LPE TH108, and (d) LPE TH54 (Dimitriadis et al., 1978).

of lifetime with distance for a single dislocation in a LPE and VPE samples(Dimitriadis et al.,1978). In all cases the lifetime tended to the bulk value at approximately one diffusion length. Table I summarized the typical lifetime reduction observed at single dislocations in various epitaxial layers (Dimitriadis et al.,1978). The temperature variation of the lifetime measured at a single dislocation and at a dislocation-free area of the samples is shown in Fig. 9 (Dimitriadis et al.,1978). It is clear that the temperature variation of the bulk lifetime is similar to that of the dislocation lifetime.

Table I. Lifetime reduction at single dislocations in different GaP epitaxial layers.

| Material | Doping (S) density ($cm^{-3}$) | lifetime reduction at dislocation |
|---|---|---|
| VPE GPR217 | $5\times10^{16}$ | 10% |
| VPE Green | $1\times10^{18}$ | 22% |
| LPE TH108 | $1\times10^{18}$ | 30% |
| LPE TH54 | $1\times10^{18}$ | 30% |

From the experimental data of the CL decay with electron beam located far from the dislocation we can determine the hole-lifetime ($\tau$) and the surface recombination velocity (s).

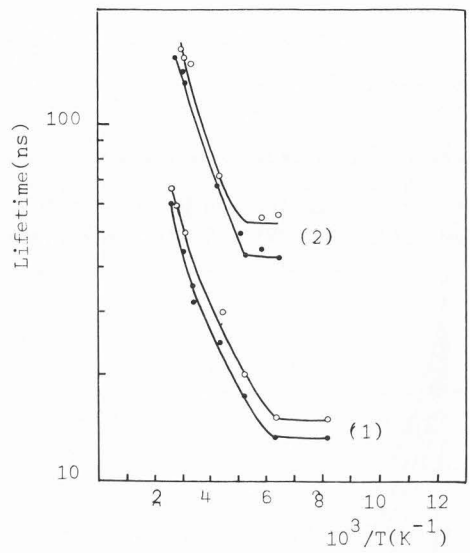


FIG.9 Temperature dependence of lifetime with the electron beam positioned at (·) and away (o) from a single dislocation in (1) VPE GPR217 and (2) LPE TH108 (Dimitriadis et al.,1978).

Figure 10 shows the $\ln(I\cdot t^{1/2})$ versus t curve obtained from the experimental data of Fig. 7. For large t a straight line is obtained, in accordance with the theory (Eq. 20), from the slope of

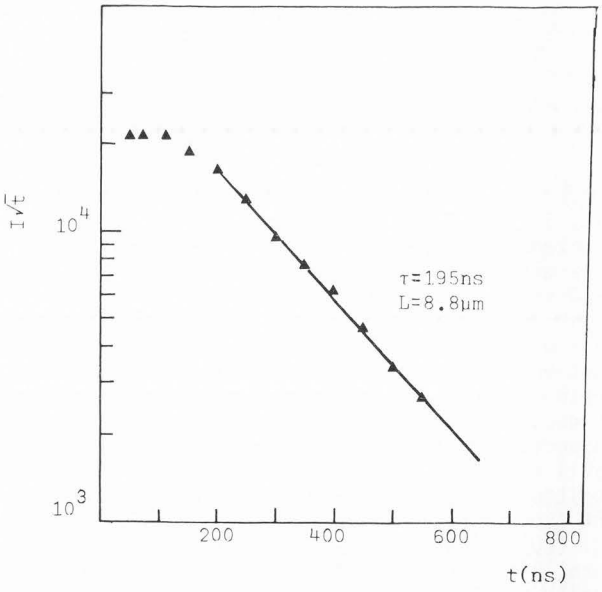


FIG. 10 Plot of $\ln(I\sqrt{t})$ versus t for the experimental data of Fig. 9 with the electron beam positioned far from the dislocation.

which we find $\tau$=195 ns. The minority carrier diffusion length L is calculated using $L^2=D\tau$, where the diffusion constant D is about 4 $cm^2s^{-1}$ in n-type GaP (Harding et al.,1976), and it is found to be L=8.8 μm. The electron penetration depth in GaP for $E_b$=25 keV is h=1.5 μm. Figure 11 (curve (a)) shows the experimental data of the CL decay

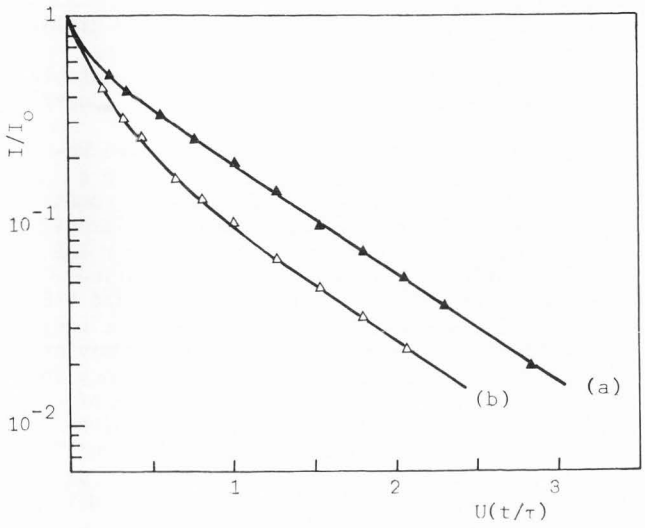


FIG. 11 Fitting of the theoretical curves $\ln(I/I_o)$ versus U with the experimental data;(a) with the electron beam positioned far from the dislocation (S=1) and (b) with the electron beam positioned at a distance 6.7 μm from the dislocation.

$I_N(t)/I_N(0)$ versus $(t/\tau)$ with the beam located far from the dislocation. Excellent fitting of the experimental points with Eq. (17) is obtained for S=1, i.e. for surface recombination velocity $s=4.5\times10^3$ cm/s. This value of s is rather small for GaP and it should be expected since the sample was polished to a mirror-like surface. Figure 11 (curve (b)) also shows the experimental data of the CL decay $I_N(t)/I_N(0)$ versus $(t/\tau)$ with the beam located at a distance $x_o=0.76$ L from the dislocation. Satisfactory fitting of the experimental points with Eq. (20) is obtained for A=0.1, i.e. for an effective dislocation radius α, that characterizes the recombination strength of the dislocation , 0.88 μm.

The value of α is incompatible with recombination taking place only at dangling bonds at the dislocation core, where α might be expected to be of the order of a few Å units. The experimental result that the lifetime reduction is smallest for the most lightly doped sample, where the depletion region radius would be expected to be largest, rules out the idea of recombination taking place at a depletion region surrounding the dislocation. Taking into account these observations and the variation of the lifetime reduction at a dislocation with material doping and growth conditions, we suggest that it is more probable that recombination takes place at a Cottrell atmosphere of impurities or defects surrounding the dislocation. The temperature dependence of dislocation recombination is very similar to that of the bulk, indicating that the recombination centres which have segregated around the dislocation are very similar to those limiting the bulk lifetime.

Nature of the Recombination Centres at Dislocations in GaP. In order to identify the nature of the recombination centres at dislocations in GaP, we investigated both as-grown dislocations and dislocations induced by plastic deformation and, also, the effect of annealing on the recombination efficiency of these defects.

The deformation was carried out with a simple bending apparatus in inert gas atmosphere at 650 °C (Dimitriadis,1983). The temperature was <680°C because above 680°C out diffusion of phosphorus occurs leaving high concentration of P-vacancies which may influence the dislocation efficiency. Black lines in CL micrographs, not seen in the same micrographs before the deformation, have been attributed to deformation-induced dislocations (Davidson et al.,1975). Annealing was carried out under vacuum of $\sim10^{-6}$ Torr in an ampoule of high purity. At annealing temperature above 680 °C losses of out-diffused P were compensated by maintaining P over-pressure. This was achieved by holding a small amount of powdered GaP at one end of the ampoule at a slightly higher temperature than the specimen temperature.

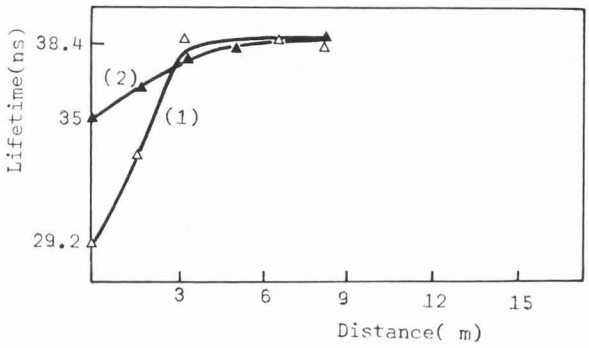


FIG. 12 Lifetime variation with distance from a single grown-in (1) and deformation-induced (2) dislocation in VPE undoped layer.

The influence on the lifetime of a single deformation-induced dislocation in comparison with a single dislocation is shown in Fig. 12. Table II shows the effect of annealing on the dislocation efficiency and on the average lifetime over a large specimen area (Dimitriadis,1983). We define the dislocation efficiency as $(1-\tau_D/\tau_B)\times100\%$, where $\tau_D$ is the lifetime measured at the dislocation and $\tau_B$ is the lifetime measured in a dislocation free-area of the sample. Table III shows the variation of the dislocation efficiency after successive removal of the surface layer in a VPE and LPE sample (Dimitriadis,1983).

From Fig. 12 and the results of Table II it is clear that:(i) The bulk lifetime in the deformed samples is nearly the same as in the control samples indicating that plastic deformation produces mainly glide-induced dislocations while the point-defect production is negligible. (ii) The deformation-induced dislocations appear to be less efficient recombination centres than the grown-in dislocations. By combining these results with the fact that the process of deformation was performed at 650 °C for about one minute,whereas the growth of the material was performed at higher

temperatures ( 800°C) for much longer time, we suggest that either impurity or native defect interactions with dislocations are the main reason for the recombination behaviour of dislocations and not the details of the dislocation structure.

Table II. Average lifetime and recombination efficiency of grown-in and deformation induced dislocations in unannealed, annealed and annealed -etched LPE TH108 GaP layer.

| Sample | Dislocation Efficiency (%) | | Average Lifetime (ns) |
|---|---|---|---|
| Unannealed | grown-in | 29 ±1.5 | 160±8 |
| | deformation -induced | 13.5±0.7 | |
| Annealed at 800°C for 24h | grown-in | 22.7±1 | 12±0.5 |
| | deformation -induced | 9±0.5 | |
| Annealed at 800°C for 24h and etched to remove a surface layer of about 4-5μm | grown-in | 14±0.7 | 26±1.5 |
| | deformation -induced | 5.5±0.3 | |

Table III. Average lifetime and dislocation efficiency with depth below the surface of the epilayer in the LPE TH108 and VPE GPR217 GaP samples.

| Sample | Depth (μm) | Average Lifetime (ns) | Dislocation Efficiency (%) |
|---|---|---|---|
| LPE GaP | 0 | 158 | 28 |
| with epilayer | 25 | 120 | 35 |
| thickness 50μm | 33.3 | 91 | 41 |
| | 41.7 | 55 | 50.5 |
| VPE GaP with | 0 | 33 | 17.8 |
| epilayer | 6 | 31.5 | 17.0 |
| thickness | 13.3 | 32 | 17.1 |
| 27.5μm | 15.2 | 31.5 | 18.4 |

Annealing of the deformed samples at 800°C reduced the average lifetime by a factor of 10, explained by assuming an effective P-vacancy production, and also reduced the dislocation efficiency due, probably, to the diffusion of the segregated impurities or native defects away from the dislocation core during the annealing. The distribution of P-vacancies created during the annealing is not known, but it can be said that a deviation from the grown-in concentration of vacancies will be established with some gradient throughout the crystal, the deviation being greatest at the surface. Because of this distribution of P-vacancies, removal of a surface layer 4-5 μm increased the lifetime by a factor of 2 and decreased the dislocation efficiency, indicating that the efficiency of dislocations follows the P-vacancy concentration. This behavior, together with the increase of the dislocation recombination efficiency with S-doping concentration, indicates that the trap responsible for the dislocation recombination is the S-donor/P-vacancy complex.

Additional support of the view that the recombination at dislocations in GaP is due to a segregation of S-donor/P-vacancy complexes comes from the analysis of the experimental results of Table III. It is clear that in the LPE layer the average lifetime decreases and the dislocation efficiency increases with depth, while in the VPE layer the lifetime and the dislocation efficiency are invariant with depth. This different behavior of the lifetime and the dislocation efficiency in the LPE and VPE layers is due to the method of material growth. The LPE layer was grown unisothermally with the temperature decreasing from the substrate towards the surface. Jordan et al. (1974) have shown that the concentration of different defects introduced into the epilayer increases with the growth temperature. Taking into account this observation, the increase of lifetime in going from the substrate towards the surface most probably results from a reduction in impurity (S-donor) incorporation or a decrease in the native defect (e.g. vacancy) concentration. The decrease of the dislocation efficiency with depth can be explained by the decrease in the concentration with depth of the S-donor/P-vacancy complexes segregated around the dislocations. The invariance of the lifetime and the dislocation efficiency with depth in the VPE layer does not contradict the above model since the VPE layer was grown isothermally and, thus, no variation in the impurity or P-vacancy concentration with depth is expected. Finally, another support of the view that the recombination at dislocations in GaP is due to a segregation of S-donor/P-vacancy complexes comes from the analysis of the CL spectra obtained from individual points on the specimen surface. Studies of the CL spectra inside and outside the dislocations in substrate materials (Tajima et al.,1978) and in epitaxial layers (Dimitriadis et al.,1978) indicated the segregation around the dislocations of a complex of VI group donors with native defects (e.g. vacancies).

Dislocation-Induced Trap Level in GaP

The lifetime measured around a single dislocation can be assumed to be controlled by recombination at uniformly distributed bulk recombination centres giving rise to a lifetime $\tau_b$ and at the dislocation giving rise to a lifetime $\tau_d$. The recombination activity of the dislocation is characterized by the lifetime $\tau_d$ which is a function of the effective radius $\alpha$ (Dimitriadis, 1984a). The measured lifetime is then given by

$$\frac{1}{\tau} = \frac{1}{\tau_b} + \frac{1}{\tau_d} \qquad (24)$$

Figure 13 shows the temperature dependence of the lifetime measured with the electron beam located in a dislocation-free area and at a single dislocation of a LPE GaP layer (Dimitriadis,1984b).

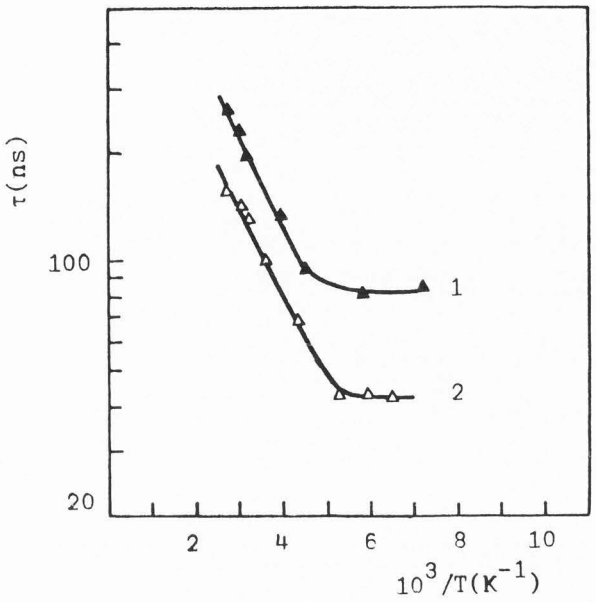


FIG.13 Temperature dependence of the minority carrier lifetime as measured from the CL decay in LPE n-type GaP layer and with the electron beam positioned (1) at a dislocation-free area of the sample and (2) at a single dislocation (Dimitriadis,1984b).

From these results and Eq.(24), the temperature dependence of the dislocation lifetime $\tau_d$ is represented in Fig.14 for a VPE and LPE sample. In both cases the lifetime $\tau_d$ decrease with decreasing the temperature and approaches a constant value at low temperatures.

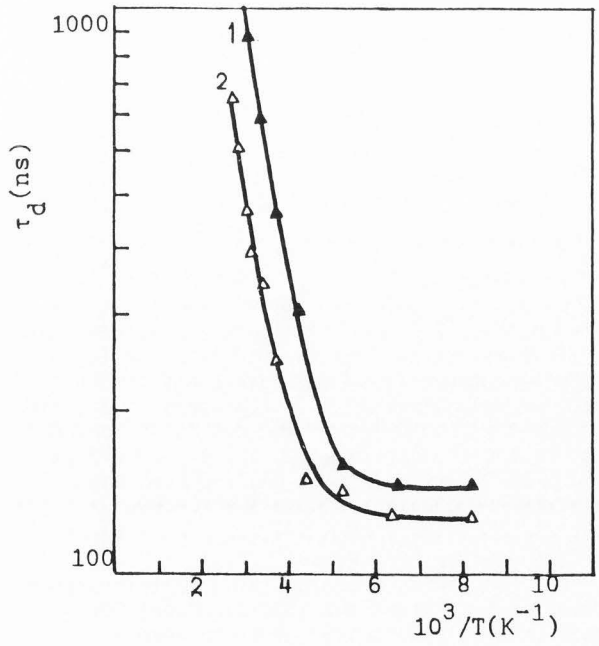


FIG.14 Temperature dependence of the dislocation lifetime in n-type (1) LPE GaP and (2) VPE GaP samples.

To explain the above temperature dependence of $\tau_d$, we assume that the non-radiative transition through dislocations is due to a single dominant recombination centre with an energy level $E_t$ and capture constant for holes $\tau_{po}^{-1}$. According to the analysis by Wessels (1975) and using Shockley-Read-Hall theory of recombination, the measured lifetime is given by

$$\tau_d=(\tau_{po}+\tau_g)+c\exp(-E_t/kT) \qquad (25)$$

where $\tau_g$ is the average time which a carrier spends in a trap. The term c is equal to $(n_i/n_o)\tau_{po}$ for a centre in the upper half of the gap and to $(p_i/n_o)\tau_{no}$ for a centre in the lower half of the gap. From Eq.(25) it is clear that $\tau_d$ decreases with T and takes a constant value $\tau_{min}=\tau_{po}+\tau_g$ at low temperatures in accordance with the experiment. Plot of $\log(\tau_d-\tau_{min})$ versus 1/T should give a straight line from the slope of which the energy level $E_t$ can be determined. Such plots, obtained from Fig.14, are shown in Fig.15. For both LPE and

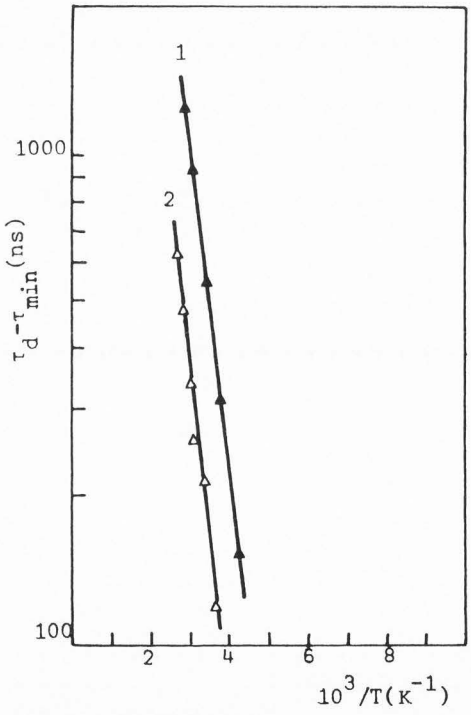


FIG.15 Temperature dependence of $\tau_d-\tau_{min}$ in n-type (1) LPE and (2) VPE GaP samples. $\tau_{min}$ is the minimum measured value of the dislocation lifetime at low temperatures (fig.14).

VPE samples we find $E_t$=0.15eV. However, we cannot determine if this level lies in the upper or lower half of the energy gap. The activation energy of 0.15eV is comparable with this found by Wessels (1975) in similar materials. Wessels attributed this level to a Cu-donor complex which was found to have an exciton binding energy of 0.16eV (Bhargava et al.,1971). By considering the results of the previous section, the last experimental result can be explained by suggesting that Cu atoms incorporate at P-sites, i.e. the recombination centres at dislocations in GaP are associated

with S-donor/Cu complexes.

Investigation of Grain Boundaries in Polycrystalline Semiconductors

Polycrystalline semiconductors are increasingly employed in the fabrication of photovoltaic devices and thin-film transistors which presented an increased interest in a number of applications such as flat panel displays and three-dimensional LSI's. However, these devices present poor performance due to excessive carrier recombination at the grain boundaries.

Considerable effort has been made for investigating the electrical properties of grain boundaries. Basic methods for characterizing the electrical activity of grain boundaries are the current-voltage (I-V), current-temperature (I-T) and capacitance-voltage (C-V) characteristics in semiconductor bicrystals(Korsh and Muller,1978; Seager and Pike,1979; Siegel et al.,1981; Truong et al.,1982; McGonigal et al.,1983; Dimitriadis et al.,1980; Siegel et al.,1986). These methods are suitable for determination of the grain boundary barrier height ($\varphi_B$) and the distribution in the energy gap of the grain boundary trap states. However, these methods give an average value of the grain boundary parameters over the whole grain boundary plane and do not allow one to estimate local variation of the grain boundary parameters.

Last years, steady-state and time-resolved EBIC methods have been used for determination of the semiconductor parameters such as lifetime ($\tau$), diffusion length (L) and effective grain boundary recombination velocity ($s_{GB}$) for the minority carriers (Leedy,1977; Berz and Kuiken,1976; Kuiken,1976; Zook,1980; Burk et al.,1983; Ioannou and Dimitriadis,1982). The use of the EBIC methods for studying grain boundaries present the advantage of local investigation of the grain boundary parameters by measuring the short-circuit current $I_{SC}$, generated by the local source of the electron beam. In this section, we describe briefly the EBIC methods developed by other authors and we, also, present a recent improvement of the steady-state EBIC method (Dimitriadis, 1985c) for investigation of grain boundaries in polycrystalline semiconductors.

The Time-Dependent Method

The geometrical configuration of the method is illustrated in Fig.16. In a polycrystalline solar cell with columnar boundaries, the p-n junction is located close to the surface and the grain boundaries are perpendicular to the surface. Electron-hole pairs are generated by an electron beam which is switched off at time t=0. Some of the carriers recombine at the grain boundary and others are collected by the p-n junction giving rise to an induced current (EBIC) in the external circuit. The grain parameters, such as the lifetime and the diffusivity of the minority carriers, and the effective recombination velocity at the grain boundary can be determined from the EBIC decay curves.

The time-dependent EBIC current near the grain boundary was analyzed by Romanowski et al. (1986). In the theoretical analysis the lumped

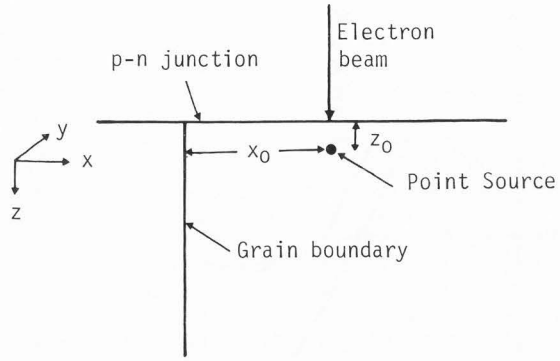


FIG.16 Geometrical configuration of the solar cell with a grain boundary and a point source excitation.

parameters of the solar cell, such as the depletion layer capacitance C, the series resistance R and the shunt circuit resistance $R_S$, were taken into account. The resistance R is, usually, much larger than the series resistance $R_S$ and may be neglected. The decay of the short-circuit current, measured with respect to the steady-state short-circuit current $I_o$, is described by the relationship (Romanowski et al.,1986)

$$I=(I_1/I_o)-(I_2/I_o)\exp(-\Omega U) \qquad (26)$$

where $U=t/\tau$, $\Omega=\tau/RC$, $I_1$ corresponds to the decay of the ideal short-circuit current (the capacitance and the series resistance are equal to zero) and $I_2$ is due to the internal parameters of the solar cell, the diffusion length and the grain boundary recombination velocity. By fitting the experimental with the theoretical EBIC decay curves, the lifetime $\tau$, the diffusion length L and the effective recombination velocity $s_{GB}$ at the grain boundary could be calculated. However, from the theoretical analysis of the EBIC decay curves, the folllowing conclusions have been obtained: (1) Variation in the value of the parameter $\Omega$ has a large effect on the EBIC decay. (2) The EBIC decay depends weakly on the distance between the grain boundary and the source if the diffusion length is less than the grain size. (3) The effective recombination velocity $s_{GB}$ at the grain boundary has only a small effect on the EBIC decay. The above conclusions show that the time-dependent EBIC method allows one to determine the lifetime of the minority carriers, while in determining the diffusion length L and the effective recombination velocity $s_{GB}$ at the grain boundary the resolution of the method is low. For this reason, the parameters L and $s_{GB}$ should be found with the steady-state EBIC method which has better resolution as described below.

The Steady-State EBIC Method

The geometrical configuration of this method is similar to that of the time-dependent EBIC method (Fig.16). A focused electron beam is incident normal to the collecting junction and is scanned along a line perpendicular to the grain boundary plane. When the electron beam is swept

across the grain boundary, the collected current decreases as a result of the enhanced carrier recombination and a contrast profile is produced.

In the past, several authors obtained expressions for contrast profiles near a grain boundary following a treatment similar to that of Zook (1980) for light beam excitation source (Zook,1980; Seager,1982; Burk et al.,1983; Donolato,1983). The expression for the EBIC response as a function of the distance $X_o$ from the grain boundary is given by (Burk et al.,1983)

$$I_{EBIC}=\frac{qG}{\pi}\int_0^{\infty}\frac{S\ 1+\exp(-Xo\ \cosh K)\ +\cosh K}{(S\ \cosh K)\ \cosh K}\times$$

$$\sinh K\times\sinh(\frac{\xi}{L}\sinh K)dK \qquad (27)$$

where $S=s_{GB}\tau/L$, G is the generation rate and $Xo=X_o/L$. Therefore, the quantitative analysis for the induced current profile at a grain boundary requires the use of a computer for numerical calculation of an integral expression (Eq.27). By fitting the theory with the experimental data of the EBIC response for distances $X_o$ greater than the penetration depth of the incident electron beam, the surface recombination velocity at the grain boundary can be determined.

In contrast to previous authors, we developed simple analytical expressions for the EBIC profiles at a grain boundary and the parameters L and $s_{GB}$ can be easily determined (Dimitriadis, 1985c). In the analysis, the following assumptions are made: (1) The injection level is low. (2) $L>>\xi$, i.e. we can consider excitation of a point source at a depth $\xi$ below the surface. This approximation is met in Si where L is a tens of μm and $\xi<5$μm up to electron beam energies 40keV. (3) The minority carriers generated by the electron beam undergo diffusion only, i.e. there is no internal electric field in the grains. (4) The depletion region width of the junction is $w<<L$ and $w<<\xi$, i.e. the junction can be considered to be lying on the semiconductor surface. (5) The thickness of the semiconductor is $d>>L$, i.e. the semiconductor can be considered as semi-infinite. (6) The influence of the grain boundary on the minority carrier distribution can be considered as a perturbation.

In order to derive an analytical expression for the EBIC profile, the grain boundary is considered as a continuous distribution of point defects in a semi-infinite plane with recombination velocity $s_{GB}$. First, we consider the results obtained by Donolato and Klann (1980) considering the influence of a point defect at the grain boundary plane on the EBIC signal as the electron beam is scanning the sample surface. Then, considering that the contribution of the total point defects of the grain boundary is additive, the influence of the grain boundary on the EBIC signal can be calculated from the corresponding expression for a point defect by integrating over the grain boundary plane.

The diode current with the beam positioned at a distance from the grain boundary can be written as

$$I_{EBIC}=I_o-I_1 \qquad (28)$$

where $I_o$ is the diode current when the beam is far from the grain boundary and $I_1$ represents the decrease of the collected current due to the grain boundary. The current $I_o$ is given by (Hackett,1972)

$$I_o=qG\exp(-\xi/L) \qquad (29)$$

For calculation of the current $I_1$ we consider a point source at the position $(x_o,0,\xi)$ and a point defect at the grain boundary at the position $(0,y,z)$. For the point defect, Donolato and Klann (1980) have shown that the current $I_1$ is given by

$$I_1=\frac{qsG}{4\pi D}\left[\frac{\exp(-r_1/L)}{r_1}-\frac{\exp(-r_2/L)}{r_2}\right] \qquad (30)$$

where s is the recombination strength of a point defect ($cm^3s^{-1}$) and

$$r_1=[x_o^2+y^2+(z-\xi)^2]^{1/2}$$
$$r_2=[x_o^2+y^2+(z+\xi)^2]^{1/2} \qquad (31)$$

Since the grain boundary is considered as a continuous distribution of point defects, the current $I_1$ for the grain boundary is obtained from (30) by integrating over the grain boundary plane after substitution of s with $s_{GB}$(cm/s). If $x_o>>\xi$ and $x_o>>L$, then after some mathematical treatment (Dimitriadis,1985c), the collected diode current normalized by the current $I_o$ is given by

$$I_{N,EBIC}=1-\frac{S_{GB}}{2\sqrt{2\pi}}\Xi\exp(\Xi)\frac{\exp(-X_o)}{\sqrt{X_o}} \qquad (32)$$

where $S_{GB}=s_{GB}/(D/L)$, $\Xi=\xi/L$, $X_o=x_o/L$. According to Eq.(32), the plot of $\ln[(1-I_{N,EBIC})x_o^{1/2}]$ versus $x_o$ should give a straight line from the slope of which the diffusion length can be obtained. The grain boundary recombination velocity can be determined from Eq. (32) provided that the parameter $\Xi$ is known. However, Eq. (32) is a first-order approximation to the grain boundary contrast which diverges for $S_{GB}\to\infty$. Therefore, for strong recombination grain boundaries, Eq.(27) may be used for the correct evaluation of the recombination velocity $s_{GB}$.

The method described above has been applied to measure the diffusion length and the grain boundary recombination velocity of a p-type polycrystalline silicon. In silicon, the generation volume can be approximated by a sphere of radius $\xi$ touching the surface with constant generation rate G ($cm^{-3}/S$). The value of $\xi$ is empirically determined by (Berz and Kuiken,1976).

$$\xi=3.84\times10^{-8}E_b^{1.75} \qquad (33)$$

where $E_b$ is in eV and $\xi$ is in μm. The EBIC experimental data were obtained from a recent work of Sundaresan et al. (1984). Figure 17 shows the

$\ell n\{(1-I_{N,EBIC})\ x_o^{1/2}\}$ versus $x_o$ curves for two typical grain boundaries as obtained at electron beam energy $E_b$=35keV. In both cases a straight line is obtained from the slope of which we find diffusion lengths 24.7 and 21.8 μm in the grains of the samples A and B, respectively.

The fitting of the experimental with theoretical curves $\ln[(1-I_{N,EBIC})\ x_o^{1/2}]$ versus $x_o$ should not be performed for small distances of the electron beam from the grain boundary for the following reasons:1) When $x_o \to 0$, the calculated EBIC signal tends to infinity, i.e. Eq. (32) is invalid and 2) within small distances of the electron beam from the grain boundary the EBIC response is not a point source response, but the response of the entire generation volume of radius ξ. Therefore, point source response can be assumed by considering the EBIC response at distances from the grain boundary greater than 2ξ.

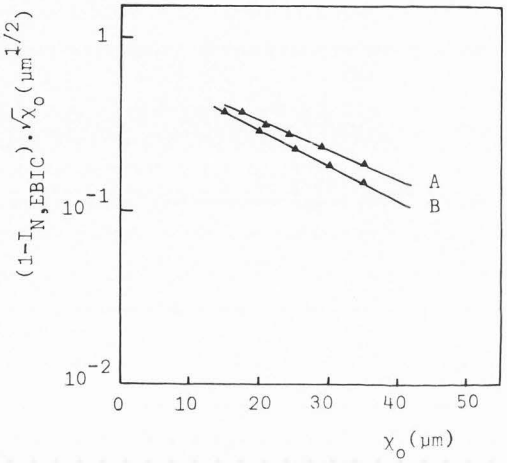


FIG. 17 $\ln[(1-I_{N,EBIC})\ x_o^{1/2}]$ versus $x_o$ plots for two typical grain boundaries in a p-type polysilicon as obtained at $E_b$=35 keV.

The grain boundary recombination velocity $s_{GB}$ is determined from Eq. (32) by using the value of ξ=3.44 μm as calculated from Eq. (33). Assuming D=25 $cm^2/s$,we find recombination velocities at the grain boundaries $2.7\times10^5$ and $2.3\times10^5$ cm/s for the cases A and B, respectively. However, the value of the parameter ξ may be different as calculated from various models, and errors in this parameter could affect the value of $s_{GB}$. Since in Silicon L>>ξ, a small change in ξ does not change significantly the ratio Ξ=ξ/L or the value of $s_{GB}$. The obtained values of L and $s_{GB}$ are in good agreement with the values obtained by other authors in similar materials by using computer-aided calculations (Seager, 1982;Burk et al.,1983;Donolato,1983).

## Conclusion

Considerable work over the last 20 years has shown that the SEM can be used effectively for assessment of semiconductor properties such as diffusion length, lifetime and dislocation density on a micrometer scale. The EBIC and CL methods described above can be used for such measurements. These methods can also be used for characterization of the electrical activity of extended defects in semiconductors such as dislocations and grain boundaries, and for measurement of the surface recombination velocity at these defects. The ability to make lifetime measurements in a micron-sized region of the semiconductor enables us to study the recombination mechanisms at individual defects.

## Acknowledgments

The author would like to acknowledge with gratitude the assistance given by Dr. S.M. Davidson in a part of this work and Prof. N.A. Economou for his helpful suggestions during the preparation of this work.

## References

Abramowitz A, Stegun IA (1965) Handbook of Mathematical Functions (Dover, New York).

Berz F, Kuiken HK (1976) Theory of lifetime measurements with the scanning electron microscope: steady-state. Solid State Electron. 19, 437-445.

Bhargava RN, Kurtz SK, Vink AT, Peters RC (1971) Spectroscopic observation of a vacancy complex in GaP. Phys. Rev. Lett. 27, 183-185.

Burk DE, Kanner S, Muyshondt JE, Shaulis DS, Russell PE (1983) Determination of surface recombination velocity at a grain boundary using electron-beam-induced-current. J. Appl. Phys. 54, 169-173.

Davidson SM, Iqbal MZ, Northrop DC (1975) SEM cathodoluminescence studies of plastically deformed GaP. Phys. Stat. Sol. (a) 29, 571-578.

Davidson SM, Rasul A (1977) A high resolution cathodoluminescence analysis system. J. Phys. E10, 43-46.

Davidson SM, (1977) Semiconductor material assessment by scanning electron microscopy. J. of Microsc. 110, 177-204.

Davidson SM, Dimitriadis CA (1980) Advances in the electrical assessment of semiconductors using the scanning electron microscope. J. Microsc. 118, 275-290.

Dimitriadis CA, Huang E, Davidson SM (1978) SEM cathodoluminescence studies of dislocation recombination in GaP. Solid State Electr. 21, 1419-1423.

Dimitriadis CA, Papadimitriou L, Valassiades O, Economou NA (1980) Electrical activity of a Σ=37 grain boundary of silicon at various temperatures. MRS Proc. on Poly-Microcrystalline and Amorphous Semiconductors, Eds. P. Pinard, S Calbitzer, Strasbourg, p. 109-114.

Dimitriadis CA (1983) Carrier recombination at dislocations in epitaxial GaP layers. Solid State Electron. 26, 633-637.

Dimitriadis CA (1984a) Recombination efficiency of single dislocations in GaP. Solid State Commun. 49, 1111-1112.

Dimitriadis CA (1984b) Temperature dependence of the hole lifetime in n-type GaP. Solid State Commun. 52, 279-281.

Dimitriadis CA (1985a) Influence of dislocations on the performance of solar cells made from large-grain polysilicon. J. Phys. D:Appl. Phys. 18, 2489-2495.

Dimitriaids CA (1985b) Influence of grain boundary recombination velocity and grain size on the minority carrier lifetime in polycrystalline semiconductors. Solid State Commun. 56, 925-927.

Dimitriadis CA (1985c) A scanning electron or

light-beam-induced current method for determination of grain boundary recombination velocity in polycrystalline semiconductors. IEEE Trans. Electr. Dev. ED-32, 1761-1766.

Dimitriadis CA (1986) Short-circuit current of polysilicon solar cells with respect to grain size and grain boundary recombination velocity. J. Appl. Phys. 59, 660-662.

Donolato C (1978) On the theory of SEM charge-collection imaging of localized defects in semiconductors. Optik 52, 19-36.

Donolato C (1979) Contrast and resolution of SEM charge-collection images of dislocations. Appl. Phys. Lett. 34, 80-81.

Donolato C, Klann H (1980) Computer stimulation of SEM electron beam induced current images. J. Appl. Phys. 51, 1624-1633.

Donolato C (1983) Theory of beam induced current characterization of grain boundaries in polycrystalline solar cell. J. Appl. Phys. 54, 1314-1322.

Everhart TE, Hoff PH (1971) Determination of kilovolt electron energy dissipation versus penetration distance in solid materials. J. Appl. Phys. 42, 5837-5846.

Figielski T (1978) Recombination at dislocations. Solid State Electron. 21, 1403-1412.

Hackett WH (1972) Electron-beam excited minority carrier diffusion profiles in semiconductors. J. Appl. Phys. 43, 1649-1654.

Harding WR, Blenkinsop ID, Wight DR (1976) Dislocation-limited minority-carrier lifetime in n-type GaP. Electron Lett. 12, 503-504.

Hastenrath M, Kubalek E (1982) Time-resolved cathodoluminescence in scanning electron microscope. Scanning Electron Microscopy, edited by O. Johari (SEM, In., Chicago, Il) p. 157.

Holt DB, Muir MD, Grant PR, Boswarwa IM (1974) Quantitative Scanning Microscopy. Academic Press.

Ioannou DE, Dimitriadis CA (1982) A SEM-EBIC minority carrier diffusion length measurement technique. IEEE Trans. Electron Dev. ED-29, 445-450.

Jakubowicz A (1987) Theory of electron beam induced current and cathodoluminescence contrasts from structural defects of semiconductor crystals: steady-state and time-resolved problems. Scanning Microscopy 1, 515-533.

Jordan AS, Von Neida AR, Caruso R, Kim CK (1974) Determination of the solidus and Gallium and Phosphorus vacancy concentrations in GaP. J. Electrochem. Soc. 121, 153-158.

Kanaya K, Okayama S (1972) Penetration and energy loss theory in solid targets. J. Phys.D 5, 43-58.

Korsh GJ, Muller RS (1978) Conduction of lightly doped polycrystalline silicon. Solid State Electron. 21, 1045-1051.

Kuiken HK (1976) Theory of lifetime measurements with the scanning electron microscope;transient analysis. Solid State Electron. 19, 447-450.

Leedy KO (1977) A bibliography on electron beam induced current analysis of semiconductor devices. Solid State Technol. 19, 45-48.

McGonigal, Thomson DJ, Shaw JG, Card HC (1983) Electronic transport at grain boundaries in silicon. Phys. Rev. B28, 5908-5922.

Myhajlenko S, Ke WK (1984) Time-resolved cathodoluminescence by delayed coincidence. J. Phys. E 17, 200-203.

Oatley CW (1972) The Scanning Electron Microscope,Part I:The Instrument. Cambridge Univ. Press.

Ourmazd A, Booker GR (1978) Influence of dissociation on individual dislocations in silicon into Shockley partials on their carrier recombination efficiency. Solid State Electron.21,1617.

Rasul A, Davidson SM (1977) A detailed study of radiative and nonradiative recombination around dislocations in GaP. Inst. Conf. Ser. No33a, 306-316.

Romanowski A, Wittry DB, Tsaur JM (1986) Analysis of the short-circuit current of a polycrystalline solar cell with excitation by a gated electron beam. J. Appl. Phys. 59, 951-957.

Seager CH, Pike GE (1979) Grain boundary states and varistor behavior in silicon bicrystals. Appl. Phys. Lett. 35, 709-711.

Seager CH (1982) The determination of grain boundary recombination rates by scanned spot excitation methods. J. Appl. Phys. 53, 5968-5971.

Siegel W, Kuhnel G, Ziegler E (1981) Electrical properties of grain boundaries in n-type and p-type GaP. Phys. Stat. Sol.(a) 64, 249-259.

Siegel W, Kuhnel G, Schneider HA (1986) Symmetrical and asymmetrical potential barriers of grain boundaries in n-type GaP. Phys. Stat. Sol. (a) 97, 609-618.

Steckenborn A (1980) Minority-carrier lifetime mapping in the SEM. J. Microsc. 118, 297-302.

Steckenborn A , Munzel H, Bimberg D (1981) Cathodoluminescence lifetime patterns of GaAs surface around dislocations. J.Lumin.24/25, 351-354.

Sundaresan R, Fossum JG, Burk DE (1984) Demonstration of excitation-dependent grain-boundary recombination velocity in polycrystalline silicon. J. Appl. Phys. 56, 964-970.

Tajima M, Okada Y, Tokumaru Y (1978) Cathodoluminescence around dislocations in an LEC-GaP crystals. Jap. J. Appl. Phys. 17, Suppl.17-1, 93-98.

Thornton PR (1968) Scanning Electron Microscopy. Publ. Chapman and Hall Ltd., London.

Titchmarsh JM, Booker GR, Harding W, Wight DR (1977) Carrier recombination at dislocations in epitaxial gallium phosphide layers. J. Mat. Sci. 12, 341-346.

Truong VK, Marchand JJ, Nodet H (1982) Grain boundaries current-voltage characteristics on Si (p) bicrystals:multi-step resonance tunneling conduction through traps. J. de Phys.C1, 43, 165-170.

Von Roosbroeck W (1955) Induced current transport in a semi-infinite semiconductor and the determination of lifetime and surface recombination velocities. J. Appl. Phys. 26, 380-391.

Wessels BW (1975) Temperature dependence of minority-carrier lifetime in vapour-grown GaP. J. Appl. Phys. 46, 2143-2146.

Zook D (1980) Effects of grain boundaries in polycrystalline solar cells. Appl. Phys. Lett. 37, 223-226.

**Editor's Note: All of the reviewer's concerns were appropriately addressed by text changes, hence there is no Discussion with Reviewers.**